HHS Public Access

Author manuscript

Biol Psychiatry. Author manuscript; available in PMC 2022 March 15.

Published in final edited form as:

Biol Psychiatry. 2021 March 15; 89(6): 600–614. doi:10.1016/j.biopsych.2020.08.026.

Critical roles of embryonic born dorsal dentate granule neurons for activity-dependent increases in BDNF, adult hippocampal neurogenesis, and anti-anxiety-like behaviors

Dong Sun[1], **Leena Milibari**[1], **Jin-Xiu Pan**[1], **Xiao Ren**[1], **Ling-Ling Yao**[1], **Yang Zhao**[1], **Chen Shen**[1], **Wen-Bing Chen**[1], **Fu-Lei Tang**[2], **Daehoon Lee**[1], **Jun-Shi Zhang**[1], **Lin Mei**[1,2,3], **Wen-Cheng Xiong**[1,2,3,*]

[1]Department of Neurosciences, School of Medicine, Case Western Reserve University, Cleveland, Ohio 44106, USA

[2]Department of Neuroscience and Regenerative Medicine, Medical College of Georgia, Augusta University, Augusta, Georgia 30912, USA

[3]Louis Stokes Cleveland Veterans Affairs Medical Center, Cleveland, Ohio 44106, USA

Abstract

Background—Dentate gyrus (DG), a “gate” that controls information flow into the hippocampus, plays important roles in regulating both cognitive (e.g., spatial learning and memory) and mood behaviors. Deficits in DG neurons contribute to the pathogenesis of not only neurological, but also psychiatric, disorders, such as anxiety disorder. Whereas DG’s function in spatial learning and memory has been extensively investigated, its role in regulating anxiety remains elusive.

Methods—Using c-fos to mark DG neuron activation, we identified a group of embryonic born dorsal DG (dDG) neurons, which were activated by anxiogenic stimuli and specifically express osteocalcin (Ocn)-Cre. We further investigated their functions in regulating anxiety and the underlying mechanisms by using a combination of chemogenetic, electrophysiological, and RNA-seq methods.

Results—The Ocn-Cre$^+$ dDG neurons were highly active in response to anxiogenic environment, but had lower excitability and less presynaptic inputs than those of Ocn-Cre$^-$ or adult born dDG neurons. Activating Ocn-Cre$^+$ dDG neurons suppressed anxiety-like behaviors and increased adult DG neurogenesis, whereas ablating or chronic inhibiting Ocn-Cre$^+$ dDG neurons exacerbated

*Corresponding author: Wen-Cheng.Xiong@case.edu, Phone: 216-368-4865, Mailing address: 2210 Circle Dr. Robbins Building, Room E722, Cleveland, Ohio 44106.

D.S. and W.-C.X. designed the project, and wrote the manuscript; D.S. performed behavioral tests, virus injection, immunostaining, western blot and data analysis; Leena M. performed data quantification and mouse genotyping; J.-X.P. and F.-L.T. made initial discovery of Ocn-Cre expression in DG; C.S. and W.-B.C did electrophysiological recordings; D.-H.L. produced rabies viruses; X.R., Y.Z. and L.-L.Y. performed RNA-seq analysis and RNA scope; Y.Z. and J.-S. Z assisted with breeding Ocn-Cre mice. L. M. and W.-C.X. helped data analysis and interpretation; W.-C.X. supervised the project.

The authors report no biomedical financial interests or potential conflicts of interest.

anxiety-like behaviors, impaired adult DG neurogenesis, and abolished activity (e.g., voluntary wheel running) induced anxiolytic effect and adult DG neurogenesis. RNA-seq screening for factors induced by activation of Ocn-Cre$^+$ dDG neurons identified brain derived neurotrophic factor (BDNF), which was required for Ocn-Cre$^+$ dDG neurons mediated anti-anxiety-like behaviors and adult DG neurogenesis.

Conclusions—These results demonstrate critical functions of Ocn-Cre$^+$ dDG neurons in suppressing anxiety-like behaviors, but promoting adult DG neurogenesis, and both functions are likely through activation of BDNF.

Keywords

Embryonic born DG neurons; Adult born DG neurons; Osteocalcin-Cre; Anxiety-like behaviors; Adult hippocampal neurogenesis; BDNF

Introduction

Anxiety disorder, the most common symptom associated with many mental illnesses, interferes with people's daily activities. Although many anti-anxiety drugs have been used clinically, they often have side effects and safety concerns (1,2). Thus, it remains of considerable interest to investigate how to alleviate anxiety and improve mental health. Abnormalities of hippocampal functions are frequently observed in patients with anxiety disorder (3,4). Several lines of animal studies have implicated hippocampus and its associated circuits in modulating anxiety-like behaviors (5–10). Silencing adult born dentate gyrus (DG) neurons or activating mature ventral DG (vDG) neurons exacerbates stress-induced anxiety-like behaviors (11), suggesting both groups of DG neurons in regulating anxiety. However, the function of embryonic born dorsal DG (dDG) neurons in this event remains unclear.

In rodents, DG is a "gate" for controlling information flow into the hippocampus. It receives the information from entorhinal cortex (EC) (synapse 1), passes it to CA3 (synapse 2), and then to CA1 (synapse 3), so called tri-synaptic hippocampal circuit (12). It thus is of interest to investigate how DG and its circuits are developed and functioned. The neural stem cells (NSCs) deriving from embryonic dentate neuro-epithelium gradually migrate to the initial DG area to generate neurons that compose the granular cell layer (GCL), as well as accumulate and form a proliferative zone, so called sub-granular zone (SGZ), where continuously gives rise to newborn dentate granule cells (DGCs) throughout life (13–16). DG thus has different layer structures, containing heterogeneous groups of neurons with different birthdays. Multiple functions of DGCs have been identified, including spatial learning and memory, epilepsy, depression and anxiety (17–22). However, how these different functions are achieved by the heterogeneous DGCs remains elusive.

Methods and Materials

Animals

Ocn-Cre (osteocalcin-Cre) mice were kindly provided by T. Clemens (Johns Hopkins Medical School, Baltimore, MD) and X. Shi (Augusta University, Augusta, GA). All the

experiments with animals were approved by the Institutional Animal Care and Use Committee of Case Western Reserve University.

Detailed Methods and Materials regarding additional animals, reagents, electrophysiological recordings, virus injections, behavioral tests and biochemical experiments are provided in Supplemental information.

Results

Selective activation of Ocn-Cre$^+$ dDGCs by anxiogenic stimuli

To understand how hippocampal neurons are involved in regulating anxiety, we first asked which group(s) of hippocampal neurons are activated in mice following anxiogenic stimulation. Mice were exposed to three established anxiety-like behavioral tests-open field test (OFT), elevated plus maze test (EPMT), or light/dark transition test (LDT) for 10 minutes (min), 1-hour (h) later, their brain samples were collected and subjected to immunostaining analysis using antibody against c-fos, an immediate early gene and a marker for neuron activation (23)(Figure S1A). As shown in Figures S1B–S1F, the c-fos$^+$ signal was detected at multiple brain regions including hippocampus and amygdala in response to the three anxiogenic environments, as compared with that of control mice in home cage. Interestingly, in hippocampus, DG, but not CA1, showed the increase of c-fos$^+$ neurons (Figures S1B–S1E); the increase of c-fos$^+$ neurons in dDG was more dramatic than that of vDG (Figures S1D and S1E); and the c-fos$^+$ dorsal DGCs (dDGCs) were largely distributed at the outer layer (Figures S1D). Notice that mice undergoing the three behavioral tests involve both locomotive activity and anxiogenic response. Thus, above results suggest that the outer layer of dDGCs appeared to be more sensitive to anxiogenic/locomotive environments than other hippocampal neurons, implicating them in regulating anxiogenic/locomotive behaviors.

To investigate functions of the outer layer of dDGCs in regulating anxiogenic/locomotive behaviors, we screened multiple Cre mouse lines in the lab for its selective expression in these neurons. The Cre-lines, including NeuroD6-Cre, CaMKII-Cre, Pomc-Cre, Nestin-Cre^{ER}, HSA-Cre, and Ocn-Cre mice, were crossed with Ai9 mice, a Cre reporter mouse line (24), respectively. As shown in Figures 1A and 1B, both NeuroD6-Cre;Ai9 and CaMKII-Cre;Ai9 mice showed high levels of tdTomato$^+$ signals not only in DG, but also in cortex, CAs, thalamus and amygdala, in line with previous reports (25,26). The Pomc-Cre driven tdTomato$^+$ neurons were selectively distributed in DG, however, they were barely distributed in the outer layer of dDG, but largely in the SGZ and inner layer of dDG (Figure 1C), in agreement with a previous report (27). Also as literature reports (28,29), the Nestin-Cre^{ER};Ai9 mice (exposed to tamoxifen at age of P60, sacrificed at age of P90) showed tdTomato$^+$ signal in NSCs and newborn neurons in the SGZ and inner layer of DG (Figure 1D); and the HSA-Cre;Ai9 mice expressed Cre/tdTomato specifically in skeletal muscles (data not shown), but not in DG/hippocampus (Figure 1E). Unexpectedly, the Ocn-Cre;Ai9 mice, a Cre mouse line largely expressed in osteoblast-lineage cells (30), showed tdTomato$^+$/Cre$^+$ signal in the brain (Figure 1F). Interestingly, the Cre$^+$ /tdTomato$^+$ neurons in Ocn-Cre;Ai9 mice was selectively distributed in the outer layer of DG, but not other hippocampal/cortical neurons (Figure 1F). Remarkably, majority of Ocn-Cre$^+$ DGCs (~94 %

of total Ocn-Cre$^+$ DGCs) were detected in dDG, representing ~33% of NeuN$^+$ dDGCs (Figures S2A–S2F). In addition to dDGCs, the tdTomato$^+$ signals in Ocn-Cre;Ai9 mice were detected in olfactory bulb (OB), cerebellum, sub-ventricular zone (SVZ), and striatum (Figure S2G). In line with previous report (30), the Ocn-Cre;Ai9 mice expressed Cre largely in the bone, but weakly in other organs, including heart, kidney, spleen, lung and liver (Figure S3). Taken together, these results suggest that Ocn-Cre may be a useful tool to investigate the functions of the outer layer of dDGCs (Figures 1G and 1H).

Next, we determined if the Ocn-Cre$^+$ dDGCs are the major group of neurons responsible to the anxiogenic or locomotive stimuli. To this end, the Ocn-Cre;Ai9 mice were exposed not only to the OFT, EPMT or LDT as described in Figure S1A, but also to the three modified tests with reduced anxiogenic factors by using a low-light (8–10 lux) in the OFT and LDT and an enclosed EPM (four closed arms) (Figure 1I). The anxiety effects were verified by the measurement of plasma levels of corticosterone (a marker of anxiogenic stress) (31) at 30 min after the behavioral tests. The plasma corticosterone levels in anxiogenic mice were much higher than that of mice exposed to non/mild anxiogenic/locomotive environments (low-light in the OFT and LDT, enclosed EPM) (Figure S4), demonstrating the anxiety induced by the anxiogenic stimuli. Co-immunostaining analysis showed increased c-fos$^+$ dDGCs in all these mice exposed to the anxiogenic or non/mild anxiogenic/locomotive stimuli, as compared with that of controls (Figures 1I–1K), indicating that dDGCs are sensitive to both types of stimuli. However, further analyses of the c-fos$^+$ signals in tdTomato$^+$ dDGCs showed that more tdTomato$^+$ neurons were activated by the anxiogenic stimuli than that by the non/mild anxiogenic/locomotive stimuli; majority (~70%) of the c-fos$^+$ neurons were tdTomato$^+$ DGCs in mice exposed to the three anxiogenic environments, whereas most (~80%) of the c-fos$^+$ DGCs were tdTomato$^-$ when mice exposed to the non/mild anxiogenic/locomotive stimuli (Figures 1I–1K). Together, these results suggest that the Ocn-Cre$^+$ dDGCs appear to be a major group of neurons to be activated by the anxiogenic stimulation.

Suppression of anxiety-like behaviors by activating Ocn-Cre$^+$ dDGCs, whereas exacerbation of anxiety-like behaviors by ablating or chronic inhibiting Ocn-Cre$^+$ dDGCs

We next examined Ocn-Cre$^+$ dDGCs' function in regulating anxiety-like behaviors. We took advantage of DREADD (designer receptors exclusively activated by designer drugs) chemogenetic method to activate Ocn-Cre$^+$ dDGCs. As shown in Figure 2A, AAV5-DIO-hM3Dq-mCherry (hM3Dq) or control viruses (AAV5-DIO-mCherry) were bilaterally injected into dDGs of Ocn-Cre mice at 6-week-old. 2 weeks later, mice were treated with CNO (2mg/kg) for 1h and subjected to behavioral tests. As expected, c-fos level was significantly increased in hM3Dq expressing Ocn-Cre$^+$ dDGCs after CNO treatment as compared with that of controls (Figure S5). However, OFT showed that both total distance and center duration time were comparable in Ocn-Cre+hM3Dq+CNO mice to those of control mice (Figure 2B), suggesting that activating Ocn-Cre$^+$ dDGCs has little effect on locomotor and exploratory activity. In contrast, EPMT showed increases in the open arm duration time and entries in Ocn-Cre+hM3Dq+CNO mice compared to that of controls (Figure 2C), suggesting that activating Ocn-Cre$^+$ dDGCs may suppress anxiety-like behavior. This view was further confirmed by LDT, which showed increased time in light

room and transition numbers after activating Ocn-Cre$^+$ dDGCs (Figure 2D). Notice that this anti-anxiety effect was mediated by Ocn-Cre$^+$ dDGCs, but not by Ocn-Cre$^+$ OB or cerebellum neurons, as activating Ocn-Cre$^+$ neurons in OB or cerebellum has little effect on anxiety-like behaviors (Figure S6).

We then asked whether Ocn-Cre$^+$ dDGCs were required for regulating anxiety-like behaviors. A Cre-dependent diphtheria toxin AAV (DTA) was bilaterally injected into dDGs of Ocn-Cre mice at 6-week-old to deplete Ocn-Cre$^+$ dDGCs. 4 weeks later, behavioral tests (e.g. OFT, EPMT and LDT) were performed (Figure 2E). As reported (32), DTA ablated ~80% of Ocn-Cre$^+$ dDGCs (Ocn-GFP$^+$) in Ocn-Cre;Ai3 mice compared to those injected with control viruses (Figure S7). Indeed, depletion of Ocn-Cre$^+$ dDGCs exacerbated anxiety-like behaviors as compared with that of control mice (Figures 2F–2H). In addition, ablating Ocn-Cre$^+$ dDGCs abolished activity (e.g., voluntary wheel running) induced anti-anxiety-like behaviors (Figures 2I–2K).

We further asked whether inhibiting Ocn-Cre$^+$ dDGCs affects anxiety-like behaviors by use of AAV5-DIO-hM4Di-mCherry (hM4Di), which expresses a double floxed Gi-coupled hM4D DREADD fused with mCherry (Figure S8A). Upon single CNO treatment, the excitability of Ocn-Cre$^+$ dDGCs was reduced in Ocn-Cre+hM4Di mice as compared with that in Ocn-Cre+mCherry mice (Figures S8A–S8C). However, little change in anxiety-like behaviors was observed in Ocn-Cre+hM4Di mice (Figures S8D–S8G). But, inhibition of the Ocn-Cre$^+$ dDGCs for 4 weeks by chronic CNO treatment (delivered in drinking water) did exacerbate the anxiety-like behaviors as compared with that of controls, and abolished activity (e.g., voluntary wheel running) induced anti-anxiety-like behaviors in EPMT (Figures S8H–S8J). Together, these results support the view for a crucial role of Ocn-Cre$^+$ dDGCs in suppressing anxiety-like behaviors.

Distinct electrophysiological properties between Ocn-Cre$^+$ and Ocn-Cre$^-$ dDGCs

Given the different response in c-fos between Ocn-Cre$^+$ and Ocn-Cre$^-$ dDGCs to the anxiogenic stimuli (Figures 1I–1K), we asked whether Ocn-Cre$^+$ dDGCs exhibit distinct electrical characteristics. To this end, ePhys-recordings were used to examine their intrinsic electrophysiological properties. As shown in Figures 3A and 3B, Ocn-Cre$^+$ dDGCs displayed comparable resting membrane potential (RMP) with that of neighboring Ocn-Cre$^-$ dDGCs. However, the frequency of action potential (AP) was lower in Ocn-Cre$^+$ dDGCs than that of Ocn-Cre$^-$ dDGCs (Figures 3C and 3D). With a 100-pA depolarizing current ramp injection, decreased AP numbers and increased rheobase were observed in Ocn-Cre$^+$ dDGCs compared to those of Ocn-Cre$^-$ dDGCs (Figures 3E–3G), indicating a lower excitability in Ocn-Cre$^+$ dDGCs than that of Ocn-Cre$^-$ dDGCs.

Ocn-Cre$^+$ dDGCs largely born at embryonic age

Notice that Ocn-Cre$^+$ dDGCs were not overlapped with retrovirus-GFP labeled newborn dDGCs, and exhibited shorter dendritic length and more primary dendrites than those of adult born dDGCs, suggesting that they may have different birthdays (Figure S9). To test this view, we performed label-retaining birth-dating experiment to determine the timing of Ocn-Cre$^+$ dDGCs' generation. First, Ocn-Cre;Ai9 mice at ages of P14 to P21 were daily

injected with 5-bromo-2'-deoxyuridine (BrdU), and sacrificed at three different ages (at P30, P60, or P120) (Figure 4A). Co-immunostaining analysis showed that $BrdU^+$ cells were mostly found in the SGZ and inner layer of DG, with a few positive cells in the outer layer, which were largely negative for tdTomato/Ocn-Cre (<2% of $tdTomato^+$ cells were $BrdU^+$) (Figures 4B–4D), suggesting that few of Ocn-Cre^+ dDGCs were born during juvenile age. Second, to determine whether Ocn-Cre^+ dDGCs were generated at earlier ages, we performed a double tracing experiment by daily injections of BrdU at E15.5 to E18.5, and daily injections of 5-ethynyl-2'-deoxyuridine (EdU) at P7 to P10, into Ocn-Cre;Ai9 mice. At P40, mice were sacrificed for analysis (Figure 4E). Interestingly, embryonically injected BrdU marked ~65% of Ocn-Cre^+ dDGCs, whereas only 1.5% of Ocn-Cre^+ dDGCs were EdU^+ (Figures 4F–4H). Third, we performed a saturate EdU labeling (50mg/kg body weight, 1time/12h) of proliferating cells from E14.5 to E18.5, which showed >80% of Ocn-Cre^+ dDGCs are EdU^+, accounting for ~40% of EdU^+ newly born dDGCs during this period (Figure 4I–4K). Together, these results suggest that Ocn-Cre^+ dDGCs are largely born at embryonic stages (Figure 4L).

Less synaptic inputs in Ocn-Cre^+ dDGCs than that of adult born dDGCs

We next applied a pseudotyped rabies virus-based retrograde monosynaptic tracing method to compare the presynaptic inputs between Ocn-Cre^+ dDGCs and adult newborn dDGCs. As shown in Figure 5A, Ocn-Cre^+ dDGCs and adult newborn dDGCs were labeled by injection of AAV1-EF1a-FLEX-GTB and RV-Syn-GTRgp viruses to express avian tumor virus receptor A (TVA) receptor and Rgp at the age of 9-week and 6-week old, respectively. At 11-week, EnvA-ΔRgp-mCherry rabies viruses were injected into the same position to infect TVA^+ neurons. The brain sections were collected at the age of 12-week to analyze the presynaptic inputs from different brain regions. Interestingly, whereas "starter cells" (GFP^+;$mCherry^+$) in Ocn-Cre^+ dDGCs were more than that in newborn dDGCs, the number of input cells ($mCherry^+$) and input ratio ($mCherry^+/GFP^+$;$mCherry^+$) in Ocn-Cre^+ dDGCs were less than those of newborn dDGCs (Figure S10), suggesting a less presynaptic connectivity in Ocn-Cre^+ dDGCs. Further analysis showed that Ocn-Cre^+ dDGCs received less presynaptic inputs than that of newborn dDGCs from multiple brain regions, including GCL, Hilus, molecular layer (ML), CAs, entorhinal cortex (EC) and medial septal (MS) (Figures 5B and 5C). Intriguingly, the Ocn-Cre^+ dDGCs mainly received inputs from local cells in GCL and projection neurons in EC, whereas newborn dDGCs received relatively balanced inputs from ML, Hilus, GCL and EC (Figure 5D). Moreover, among the local presynaptic inputs ($mCherry^+$) in DG area, more $CaMKII^+$;$mCherry^+$ excitatory neurons, comparable PV^+;$mCherry^+$ interneurons, but less DCX^+;$mCherry^+$ immature neurons were observed in Ocn-Cre^+ dDGCs than those of newborn dDGCs (Figures 5E–5G). Together, these results suggest that Ocn-Cre^+ dDGCs receive less presynaptic inputs than that of newborn dDGCs, with a distinct ratio of presynaptic inputs from different cell types in DG as compared with that of newborn dDGCs.

Increased adult DG neurogenesis by activating Ocn-Cre^+ dDGCs, whereas decreased adult DG neurogenesis by ablating or inhibting Ocn-Cre^+ dDGCs

Given the interaction between embryonic born and newborn dDGCs, we asked whether Ocn-Cre^+ dDGCs regulate adult DG neurogenesis. To this end, the Ocn-Cre mice injected with

mCherry or hM3Dq viruses in dDG at 6-week-old, and treated with CNO (2mg/kg) at 8-week-old for 1 h, were injected with BrdU (1 time/4 h, 4x). Mice were sacrificed 12 h or 1-week post the last BrdU injection (Figure 6A). Interestingly, increases in $BrdU^+$ cells, $Mcm2^+$ transient amplifying NSCs/NPCs, and DCX^+ immature neurons were all detected in dDG of Ocn-Cre+hM3Dq+CNO mice as compared with those of controls (Figures 6B and 6C), suggesting that activation of Ocn-Cre^+ dDGCs promotes adult DG neurogenesis.

Next, we determined whether Ocn-Cre^+ dDGCs are required for adult DG neurogenesis. To this end, the Ocn-Cre mice injected with control or DTA viruses into dDG (at age of 6-week-old) and BrdU (1 time/4 h, 4 x) (at age of 10-week-old) were sacrificed 12 h post last BrdU injection (Figure 6D). The density of $BrdU^+$ cells, $Mcm2^+$ transient amplifying NSCs/NPCs, and DCX^+ immature neurons were all lower in dDG of Ocn-Cre+DTA mice than those of controls (Figures 6E and 6F), demonstrating a necessity of Ocn-Cre^+ dDGCs for adult DG neurogenesis. In further supporting this view was the observation that the acute inhibition of Ocn-Cre^+ dDGCs in Ocn-Cre+hM4Di+CNO mice reduced adult DG neurogenesis as compared with that in Ocn-Cre+mCherry+CNO mice (Figures S11A–S11C).

Given that activity (e.g., voluntary wheel running) promotes adult DG neurogenesis (33,34), and voluntary wheel running mainly activates excitatory neurons rather than GABAergic interneurons in DG (35), we asked whether Ocn-Cre^+ dDGCs are required for this event. The Ocn-Cre mice injected with control or DTA viruses were given the access to voluntary wheel running for 1 week (Figure 6G). Whereas control mice after voluntary wheel running showed elevated DG neurogenesis, mice with depletion of Ocn-Cre^+ dDGCs (by DTA) exhibited little to no change in $BrdU^+$ cell density and DCX^+ neuron density with or without voluntary wheel running (Figures 6H and 6I). Furthermore, inhibiting Ocn-Cre^+ dDGCs (by hM4Di+CNO) abolished activity induced adult DG neurogenesis (Figures S11D–S11F). These results thus demonstrate a critical role of Ocn-Cre^+ dDGCs in activity induced adult DG neurogenesis.

Ocn-Cre^+ dDGCs, a key cellular source for activity induced hippocampal BDNF

To investigate mechanisms by which Ocn-Cre^+ dDGCs suppress anxiety-like behaviors and promote adult DG neurogenesis, we performed RNA-seq analysis to identify differentially expressed genes in hippocampus of Ocn-Cre+mCherry+CNO and Ocn-Cre+hM3Dq+CNO mice (Figure 7A). As shown in Table S1, the acute activation of Ocn-Cre^+ dDGCs led to 366 upregulated and 344 downregulated genes as compared with controls. Further analysis of these genes showed that in addition to immediate early genes (e.g., fos, Arc), one of the most upregulated genes is brain derived neurotrophic factor (BDNF) (Figures 7B and 7C), a factor known to be critical for anti-anxiety-like behaviors and promoting adult DG neurogenesis (36–38). The BDNF-increase in hippocampus of Ocn-Cre+hM3Dq+CNO mice was further confirmed by RNA scope, RT-PCR, and Western blot analyses (Figures 7D and 7E, S12A and S12B). Additionally, the level of phosphorylated TrkB (p-TrkB), a down-stream signaling induced by BDNF, was significantly increased in the SGZ region of dDG upon activation of Ocn-Cre^+ dDGCs (Figures S12C and S12D). Moreover, the downstream signaling pathway of BDNF-TrkB, phospho-Akt2/3/3 (p-Akt2/3/3), but not phospho-Erk2/3

(p-Erk2/3), was increased after activating Ocn-Cre$^+$ dDGCs (Figures S12E and S12F). Thus, these results lead to the hypothesis that Ocn-Cre$^+$ dDGCs regulate anxiety-like behaviors and adult DG neurogenesis likely by BDNF pathway.

We next asked whether Ocn-Cre$^+$ dDGCs are required for activity (e.g., voluntary wheel running) induced BDNF-increase in hippocampus. The hippocampal sections from Ocn-Cre mice injected with control or DTA viruses were subjected to RNA-scope analysis of BDNF. BDNF mRNAs in hippocampus, including DG, CA1 and CA3, were elevated in control mice after voluntary wheel running (Figures 7F–7H), in line with previous reports (39,40). However, the BDNF-increase was abolished in DTA expressing/Ocn-Cre$^+$ dDGCs depleted mice (Figures 7F–7H). Furthermore, the activity-induced BDNF-increase was impaired after inhibiting Ocn-Cre$^+$ dDGCs (by hM4Di+CNO) (Figure S13). These results thus demonstrate the necessity of activation of Ocn-Cre$^+$ dDGCs for activity-induced BDNF expression.

Requirement of BDNF in hippocampus for Ocn-Cre$^+$ dDGC induced anti-anxiety and adult DG neurogenesis

To determine if BDNF is required for activating Ocn-Cre$^+$ dDGCs induced anti-anxiety and adult DG neurogenesis, BDNF expression in hippocampus was knocked down by injecting lentiviral particles encoding BDNF-shRNA for 2 weeks (Figure 8A). As expected, the hippocampal BDNF expression was increased in Ocn-Cre+hM3Dq+scramble-shRNA+CNO mice, but not in Ocn-Cre+hM3Dq+BDNF-shRNA+CNO mice (Figure 8B). EPMT and LDT showed that decreases of anxiety-like behaviors in both Ocn-Cre+hM3Dq and Ocn-Cre +hM3Dq+scramble-shRNA mice after CNO treatment (Figures 8C–8E). However, suppressing BDNF expression abolished these anti-anxiety-like responses (Figures 8C–8E), suggesting that the BDNF-increase in hippocampus mediates the activation of Ocn-Cre$^+$ dDGCs induced anxiolytic effect.

Next, we examined adult DG neurogenesis by immunostaining analyses of BrdU$^+$ and DCX $^+$ cell densities (Figures 8F and 8G). In comparison with the control mice, both BrdU$^+$ cells and DCX$^+$ immature neurons were increased in Ocn-Cre+hM3Dq+CNO and Ocn-Cre +hM3Dq+scramble-shRNA+CNO mice, but not in Ocn-Cre+hM3Dq+BDNF-shRNA+CNO mice (Figure 8H), suggesting a necessity of BDNF for activating Ocn-Cre$^+$ dDGCs induced adult DG neurogenesis. Furthermore, knocking down BDNF in hippocampus abolished the increase of p-TrkB and p-Akt2/3/3 induced by activation of Ocn-Cre$^+$ dDGCs (Figure S14), suggesting that TrkB-Akt signaling may be a critical pathway to underlie BDNF-induced adult DG neurogenesis in Ocn-Cre+hM3Dq+CNO mice.

Taken together, these results demonstrate that both the anti-anxiety like behaviors and adult DG neurogenesis induced by activation of Ocn-Cre$^+$ dDGCs are likely mediated by the increase of hippocampal BDNF expression (Figure 8I).

Discussion

Here, we identified the Ocn-Cre mouse line, not only marks osteoblast-lineage cells, but also selectively labels the embryonic born dDGCs. Using this mouse line, we have found that the embryonic born Ocn-Cre$^+$ dDGCs play critical roles in preventing anxiety-like behaviors

and in increasing adult DG neurogenesis. Both functions appear to be mediated by the activity-induced BDNF expression in these neurons.

To study DG's function, multiple Cre lines have been used, including NeuroD6-Cre, CaMKII-Cre, Pomc-Cre, and Nestin-Cre^{ER} (41–44). Among these Cre lines, Pomc-Cre is known to selectively express Cre in DG, however, it mainly labels postnatal newborn DGCs (27). Our studies identify Ocn-Cre to be selectively expressed in the outer layer of DG, suggesting that Ocn-Cre could be a new tool in investigating dDGCs' function (Figures 1F and S2). However, it needs to be cautious to make any conclusion regarding Ocn-Cre^{+} dDGCs' function, because Ocn-Cre is also highly expressed in osteoblast lineage cells (30,45,46), as well as non-osteoblastic cells, such as CAR cells (47).

Our results that the embryonic born Ocn-Cre^{+} dDGCs exhibit distinct features from those of adult born dDGCs (Figures 1D and 1F, 3, 5 and S9D–S9G) support the "outside-in" DG layering pattern (48), and in line with the view for neuron birthdate could determine the intrinsic properties of DGCs, including neuronal morphology, excitability and connectivity (49–51). Interestingly, while Ocn-Cre^{+} dDGCs have lower excitability and receive less presynaptic inputs than those of Ocn-Cre^{-} or adult newborn dDGCs, they are more sensitive than adult born or Ocn-Cre^{-} dDGCs in respond to the anxiogenic stimuli (Figures 1I–1K), implicating that their circuitry might be more sensitive to the anxiogenic stimuli. Notice the report that the adult born DGCs are activated during learning a novel task; the developmental born DGCs are activated for discriminating dissimilar contexts (52). Our results that dDGCs in the suprapyramidal blade are activated by the anxiogenic stimuli (Figure S1B) are also in line with the report that DGCs in the suprapyramidal blade often show a higher neuronal activity than that in the infrapyramidal blade (53). These observations support the view that DG neurons with different birthdays could have distinct functions.

Several lines of evidence suggest that the Ocn-Cre^{+} dDGCs play important roles in suppressing anxiety-like behaviors. First, Ocn-Cre^{+} dDGCs were selectively activated by anxiogenic stimuli, but not non/mild anxiogenic environments (Figures 1I–1K). Second, activating Ocn-Cre^{+} dDGCs suppressed anxiety-like behaviors, whereas ablating or chronic inhibiting Ocn-Cre^{+} dDGCs exacerbated anxiety-like behaviors (Figures 2A–2H, S8H–S8J). Third, ablating or chronic inhibiting Ocn-Cre^{+} dDGCs abolished activity (e.g., voluntary wheel running) induced anti-anxiety-like behaviors (Figures 2I–2K, S8H–S8J). Additionally, Ocn-Cre^{+} dDGCs play a critical role in adult DG neurogenesis (Figures 6 and S11), an event associated with mood regulation, including anxiety (54,55). Because there are controversial reports regarding new born neurons' function in regulating anxiety (55–58), and the anti-anxiety-like behavior by activating Ocn-Cre^{+} dDGCs appears to be a quick response (Figures 2A–2D), we speculate that this Ocn-Cre^{+} dDGCs' function may be not due to the increase of adult newborn neurons, and both functions (anti-anxiety and increase of adult DG neurogenesis) by Ocn-Cre^{+} dDGCs may be through two parallel pathways. Notice the reports that optogenetic activation of Pomc-Cre^{+} DGCs in dDG or vDG suppresses anxiety-like behaviors, but Pomc-Cre^{+} dDGCs are more likely to drive exploratory behavior (59); activating newborn neurons suppresses depression and anxiety-like behaviors in baseline conditions (60) and inhibiting adult-born neurons in the vDG promotes susceptibility to

social defeat stress (11). Our results are in line with these observations, suggesting that different groups of DGCs could be activated by different conditions and thus contribute to the distinct anti-anxiety functions.

How does activation of Ocn-Cre$^+$ dDGCs mediate anti-anxiety like behaviors and promote adult DG neurogenesis? Our results suggest that BDNF is a critical mediator for both events. BDNF mRNA and protein levels in hippocampus are rapidly increased following the activation of Ocn-Cre$^+$ dDGCs (Figures 7A–7E, S12A–S12B). BDNF induced signaling (e.g., p-TrkB and p-Akt) is elevated in the DG after activation of Ocn-Cre$^+$ dDGCs (Figures S12C–12F). Knocking down BDNF expression in hippocampus abolished activation of Ocn-Cre$^+$ dDGCs induced both functions of anti-anxiety and promotion of adult DG neurogenesis, and BDNF signaling (increases in p-TrkB and p-Akt) (Figures 8 and S14). These observations are in line with the literature reports that BDNF, a neuronal activity induced immediate early gene (61), plays a crucial role in promoting adult DG neurogenesis and preventing anxiety disorders (36,37,62).

In summary, our results provide evidence for Ocn-Cre as a new tool to investigate the functions of embryonic born dDGCs. These Ocn-Cre$^+$ dDGCs exhibit distinct morphological and electrophysiological features, and play essential roles in neuronal activity induced BDNF expression, anti-anxiety-like behaviors, and adult DG neurogenesis.

Supplementary Material

Refer to Web version on PubMed Central for supplementary material.

Acknowledgements and Disclosures

This study was supported by the grant from the National Institutes of Health [AG045781 and AG051773 to WCX, NS082007, NS090083, AG051510, and MH083317 to LM]. We thank Dr. Ben W. Strowbridge (Department of Neurosciences, CWRU), and members in Drs. Xiong and Mei laboratories for helpful discussions and suggestions.

Reference

1. Bandelow B, Michaelis S, and Wedekind D, Treatment of anxiety disorders. Dialogues Clin Neurosci, 2017 19(2): p. 93–107. [PubMed: 28867934]
2. Farach FJ, Pruitt LD, Jun JJ, Jerud AB, Zoellner LA, and Roy-Byrne PP, Pharmacological treatment of anxiety disorders: current treatments and future directions. J Anxiety Disord, 2012 26(8): p. 833–43. [PubMed: 23023162]
3. Cha J, Greenberg T, Song I, Blair Simpson H, Posner J, and Mujica-Parodi LR, Abnormal hippocampal structure and function in clinical anxiety and comorbid depression. Hippocampus, 2016 26(5): p. 545–53. [PubMed: 26743454]
4. Machado-de-Sousa JP, Osorio Fde L, Jackowski AP, Bressan RA, Chagas MH, Torro-Alves N, et al., Increased amygdalar and hippocampal volumes in young adults with social anxiety. PLoS One, 2014 9(2): p. e88523. [PubMed: 24523911]
5. Felix-Ortiz AC, Beyeler A, Seo C, Leppla CA, Wildes CP, and Tye KM, BLA to vHPC inputs modulate anxiety-related behaviors. Neuron, 2013 79(4): p. 658–64. [PubMed: 23972595]
6. Jimenez JC, Su K, Goldberg AR, Luna VM, Biane JS, Ordek G, et al., Anxiety Cells in a Hippocampal-Hypothalamic Circuit. Neuron, 2018 97(3): p. 670–683 e6. [PubMed: 29397273]
7. Shin LM and Liberzon I, The neurocircuitry of fear, stress, and anxiety disorders. Neuropsychopharmacology, 2010 35(1): p. 169–91. [PubMed: 19625997]

8. Calhoon GG and Tye KM, Resolving the neural circuits of anxiety. Nat Neurosci, 2015 18(10): p. 1394–404. [PubMed: 26404714]

9. Eren-Kocak E, Turner CA, Watson SJ, and Akil H, Short-hairpin RNA silencing of endogenous fibroblast growth factor 2 in rat hippocampus increases anxiety behavior. Biol Psychiatry, 2011 69(6): p. 534–40. [PubMed: 21215386]

10. Salvi SS, Pati S, Chaudhari PR, Tiwari P, Banerjee T, and Vaidya VA, Acute Chemogenetic Activation of CamKIIalpha-Positive Forebrain Excitatory Neurons Regulates Anxiety-Like Behaviour in Mice. Front Behav Neurosci, 2019 13: p. 249. [PubMed: 31736725]

11. Anacker C, Luna VM, Stevens GS, Millette A, Shores R, Jimenez JC, et al., Hippocampal neurogenesis confers stress resilience by inhibiting the ventral dentate gyrus. Nature, 2018 559(7712): p. 98–102. [PubMed: 29950730]

12. van Strien NM, Cappaert NL, and Witter MP, The anatomy of memory: an interactive overview of the parahippocampal-hippocampal network. Nat Rev Neurosci, 2009 10(4): p. 272–82. [PubMed: 19300446]

13. Khalaf-Nazzal R and Francis F, Hippocampal development - old and new findings. Neuroscience, 2013 248: p. 225–42. [PubMed: 23756184]

14. Rickmann M, Amaral DG, and Cowan WM, Organization of radial glial cells during the development of the rat dentate gyrus. J Comp Neurol, 1987 264(4): p. 449–79. [PubMed: 3680638]

15. Urban N and Guillemot F, Neurogenesis in the embryonic and adult brain: same regulators, different roles. Front Cell Neurosci, 2014 8: p. 396. [PubMed: 25505873]

16. Kempermann G and Gage FH, New nerve cells for the adult brain. Sci Am, 1999 280(5): p. 48–53. [PubMed: 10231988]

17. Snyder JS, Hong NS, McDonald RJ, and Wojtowicz JM, A role for adult neurogenesis in spatial long-term memory. Neuroscience, 2005 130(4): p. 843–52. [PubMed: 15652983]

18. Yau SY, Li A, and So KF, Involvement of Adult Hippocampal Neurogenesis in Learning and Forgetting. Neural Plast, 2015 2015: p. 717958. [PubMed: 26380120]

19. Clelland CD, Choi M, Romberg C, Clemenson GD Jr., Fragniere A, Tyers P, et al., A functional role for adult hippocampal neurogenesis in spatial pattern separation. Science, 2009 325(5937): p. 210–3. [PubMed: 19590004]

20. Bergami M, Berninger B, and Canossa M, Conditional deletion of TrkB alters adult hippocampal neurogenesis and anxiety-related behavior. Commun Integr Biol, 2009 2(1): p. 14–6. [PubMed: 19704856]

21. Jessberger S and Parent JM, Epilepsy and Adult Neurogenesis. Cold Spring Harb Perspect Biol, 2015 7(12).

22. Boldrini M, Galfalvy H, Dwork AJ, Rosoklija GB, Trencevska-Ivanovska I, Pavlovski G, et al., Resilience Is Associated With Larger Dentate Gyrus, While Suicide Decedents With Major Depressive Disorder Have Fewer Granule Neurons. Biol Psychiatry, 2019 85(10): p. 850–862. [PubMed: 30819514]

23. Bullitt E, Expression of c-fos-like protein as a marker for neuronal activity following noxious stimulation in the rat. J Comp Neurol, 1990 296(4): p. 517–30. [PubMed: 2113539]

24. Madisen L, Zwingman TA, Sunkin SM, Oh SW, Zariwala HA, Gu H, et al., A robust and high-throughput Cre reporting and characterization system for the whole mouse brain. Nat Neurosci, 2010 13(1): p. 133–40. [PubMed: 20023653]

25. Goebbels S, Bormuth I, Bode U, Hermanson O, Schwab MH, and Nave KA, Genetic targeting of principal neurons in neocortex and hippocampus of NEX-Cre mice. Genesis, 2006 44(12): p. 611–21. [PubMed: 17146780]

26. Tsien JZ, Chen DF, Gerber D, Tom C, Mercer EH, Anderson DJ, et al., Subregion- and cell type-restricted gene knockout in mouse brain. Cell, 1996 87(7): p. 1317–26. [PubMed: 8980237]

27. Gao X, Arlotta P, Macklis JD, and Chen J, Conditional knock-out of beta-catenin in postnatal-born dentate gyrus granule neurons results in dendritic malformation. J Neurosci, 2007 27(52): p. 14317–25. [PubMed: 18160639]

28. Miniou P, Tiziano D, Frugier T, Roblot N, Le Meur M, and Melki J, Gene targeting restricted to mouse striated muscle lineage. Nucleic Acids Res, 1999 27(19): p. e27. [PubMed: 10481039]

29. Lagace DC, Whitman MC, Noonan MA, Ables JL, DeCarolis NA, Arguello AA, et al., Dynamic contribution of nestin-expressing stem cells to adult neurogenesis. J Neurosci, 2007 27(46): p. 12623–9. [PubMed: 18003841]
30. Zhang M, Xuan S, Bouxsein ML, von Stechow D, Akeno N, Faugere MC, et al., Osteoblast-specific knockout of the insulin-like growth factor (IGF) receptor gene reveals an essential role of IGF signaling in bone matrix mineralization. J Biol Chem, 2002 277(46): p. 44005–12. [PubMed: 12215457]
31. Rodgers RJ, Haller J, Holmes A, Halasz J, Walton TJ, and Brain PF, Corticosterone response to the plus-maze: high correlation with risk assessment in rats and mice. Physiol Behav, 1999 68(1–2): p. 47–53. [PubMed: 10627061]
32. Wu Z, Autry AE, Bergan JF, Watabe-Uchida M, and Dulac CG, Galanin neurons in the medial preoptic area govern parental behaviour. Nature, 2014 509(7500): p. 325–30. [PubMed: 24828191]
33. Gremmelspacher T, Gerlach J, Hubbe A, Haas CA, and Haussler U, Neurogenic Processes Are Induced by Very Short Periods of Voluntary Wheel-Running in Male Mice. Front Neurosci, 2017 11: p. 385. [PubMed: 28751854]
34. Zang J, Liu Y, Li W, Xiao D, Zhang Y, Luo Y, et al., Voluntary exercise increases adult hippocampal neurogenesis by increasing GSK-3beta activity in mice. Neuroscience, 2017 354: p. 122–135. [PubMed: 28456716]
35. Dong J, Pan YB, Wu XR, He LN, Liu XD, Feng DF, et al., A neuronal molecular switch through cell-cell contact that regulates quiescent neural stem cells. Sci Adv, 2019 5(2): p. eaav4416. [PubMed: 30820459]
36. Chen ZY, Jing D, Bath KG, Ieraci A, Khan T, Siao CJ, et al., Genetic variant BDNF (Val66Met) polymorphism alters anxiety-related behavior. Science, 2006 314(5796): p. 140–3. [PubMed: 17023662]
37. Scharfman H, Goodman J, Macleod A, Phani S, Antonelli C, and Croll S, Increased neurogenesis and the ectopic granule cells after intrahippocampal BDNF infusion in adult rats. Exp Neurol, 2005 192(2): p. 348–56. [PubMed: 15755552]
38. Martinowich K, Manji H, and Lu B, New insights into BDNF function in depression and anxiety. Nat Neurosci, 2007 10(9): p. 1089–93. [PubMed: 17726474]
39. Duman CH, Schlesinger L, Russell DS, and Duman RS, Voluntary exercise produces antidepressant and anxiolytic behavioral effects in mice. Brain Res, 2008 1199: p. 148–58. [PubMed: 18267317]
40. Wrann CD, White JP, Salogiannnis J, Laznik-Bogoslavski D, Wu J, Ma D, et al., Exercise induces hippocampal BDNF through a PGC-1alpha/FNDC5 pathway. Cell Metab, 2013 18(5): p. 649–59. [PubMed: 24120943]
41. Li G, Fang L, Fernandez G, and Pleasure SJ, The ventral hippocampus is the embryonic origin for adult neural stem cells in the dentate gyrus. Neuron, 2013 78(4): p. 658–72. [PubMed: 23643936]
42. Minichiello L, Korte M, Wolfer D, Kuhn R, Unsicker K, Cestari V, et al., Essential role for TrkB receptors in hippocampus-mediated learning. Neuron, 1999 24(2): p. 401–14. [PubMed: 10571233]
43. Feng S, Shi T, Qiu J, Yang H, Wu Y, Zhou W, et al., Notch1 deficiency in postnatal neural progenitor cells in the dentate gyrus leads to emotional and cognitive impairment. FASEB J, 2017 31(10): p. 4347–4358. [PubMed: 28611114]
44. Lagace DC, Benavides DR, Kansy JW, Mapelli M, Greengard P, Bibb JA, et al., Cdk5 is essential for adult hippocampal neurogenesis. Proc Natl Acad Sci U S A, 2008 105(47): p. 18567–71. [PubMed: 19017796]
45. Xiong L, Jung JU, Wu H, Xia WF, Pan JX, Shen C, et al., Lrp4 in osteoblasts suppresses bone formation and promotes osteoclastogenesis and bone resorption. Proc Natl Acad Sci U S A, 2015 112(11): p. 3487–92. [PubMed: 25733894]
46. Xiong L, Jung JU, Guo HH, Pan JX, Sun XD, Mei L, et al., Osteoblastic Lrp4 promotes osteoclastogenesis by regulating ATP release and adenosine-A2AR signaling. J Cell Biol, 2017 216(3): p. 761–778. [PubMed: 28193701]

47. Zhang J and Link DC, Targeting of Mesenchymal Stromal Cells by Cre-Recombinase Transgenes Commonly Used to Target Osteoblast Lineage Cells. J Bone Miner Res, 2016 31(11): p. 2001–2007. [PubMed: 27237054]

48. Mathews EA, Morgenstern NA, Piatti VC, Zhao C, Jessberger S, Schinder AF, et al., A distinctive layering pattern of mouse dentate granule cells is generated by developmental and adult neurogenesis. J Comp Neurol, 2010 518(22): p. 4479–90. [PubMed: 20886617]

49. Save L, Baude A, and Cossart R, Temporal Embryonic Origin Critically Determines Cellular Physiology in the Dentate Gyrus. Cereb Cortex, 2019 29(6): p. 2639–2652. [PubMed: 29878074]

50. Kerloch T, Clavreul S, Goron A, Abrous DN, and Pacary E, Dentate Granule Neurons Generated During Perinatal Life Display Distinct Morphological Features Compared With Later-Born Neurons in the Mouse Hippocampus. Cereb Cortex, 2019 29(8): p. 3527–3539. [PubMed: 30215686]

51. Kerloch T, Clavreul S, Goron A, Abrous DN, and Pacary E, Dentate Granule Neurons Generated During Perinatal Life Display Distinct Morphological Features Compared With Later-Born Neurons in the Mouse Hippocampus. Cereb Cortex, 2018.

52. Tronel S, Lemaire V, Charrier V, Montaron MF, and Abrous DN, Influence of ontogenetic age on the role of dentate granule neurons. Brain Struct Funct, 2015 220(2): p. 645–61. [PubMed: 24510284]

53. Schmidt B, Marrone DF, and Markus EJ, Disambiguating the similar: the dentate gyrus and pattern separation. Behav Brain Res, 2012 226(1): p. 56–65. [PubMed: 21907247]

54. Hill AS, Sahay A, and Hen R, Increasing Adult Hippocampal Neurogenesis is Sufficient to Reduce Anxiety and Depression-Like Behaviors. Neuropsychopharmacology, 2015 40(10): p. 2368–78. [PubMed: 25833129]

55. Revest JM, Dupret D, Koehl M, Funk-Reiter C, Grosjean N, Piazza PV, et al., Adult hippocampal neurogenesis is involved in anxiety-related behaviors. Mol Psychiatry, 2009 14(10): p. 959–67. [PubMed: 19255582]

56. Petrik D, Lagace DC, and Eisch AJ, The neurogenesis hypothesis of affective and anxiety disorders: are we mistaking the scaffolding for the building? Neuropharmacology, 2012 62(1): p. 21–34. [PubMed: 21945290]

57. Saxe MD, Battaglia F, Wang JW, Malleret G, David DJ, Monckton JE, et al., Ablation of hippocampal neurogenesis impairs contextual fear conditioning and synaptic plasticity in the dentate gyrus. Proc Natl Acad Sci U S A, 2006 103(46): p. 17501–6. [PubMed: 17088541]

58. Onksen JL, Brown EJ, and Blendy JA, Selective deletion of a cell cycle checkpoint kinase (ATR) reduces neurogenesis and alters responses in rodent models of behavioral affect. Neuropsychopharmacology, 2011 36(5): p. 960–9. [PubMed: 21248719]

59. Kheirbek MA, Drew LJ, Burghardt NS, Costantini DO, Tannenholz L, Ahmari SE, et al., Differential control of learning and anxiety along the dorsoventral axis of the dentate gyrus. Neuron, 2013 77(5): p. 955–68. [PubMed: 23473324]

60. Tunc-Ozcan E, Peng CY, Zhu Y, Dunlop SR, Contractor A, and Kessler JA, Activating newborn neurons suppresses depression and anxiety-like behaviors. Nat Commun, 2019 10(1): p. 3768. [PubMed: 31434877]

61. Hughes P, Beilharz E, Gluckman P, and Dragunow M, Brain-derived neurotrophic factor is induced as an immediate early gene following N-methyl-D-aspartate receptor activation. Neuroscience, 1993 57(2): p. 319–28. [PubMed: 8115041]

62. Liu PZ and Nusslock R, Exercise-Mediated Neurogenesis in the Hippocampus via BDNF. Front Neurosci, 2018 12: p. 52. [PubMed: 29467613]

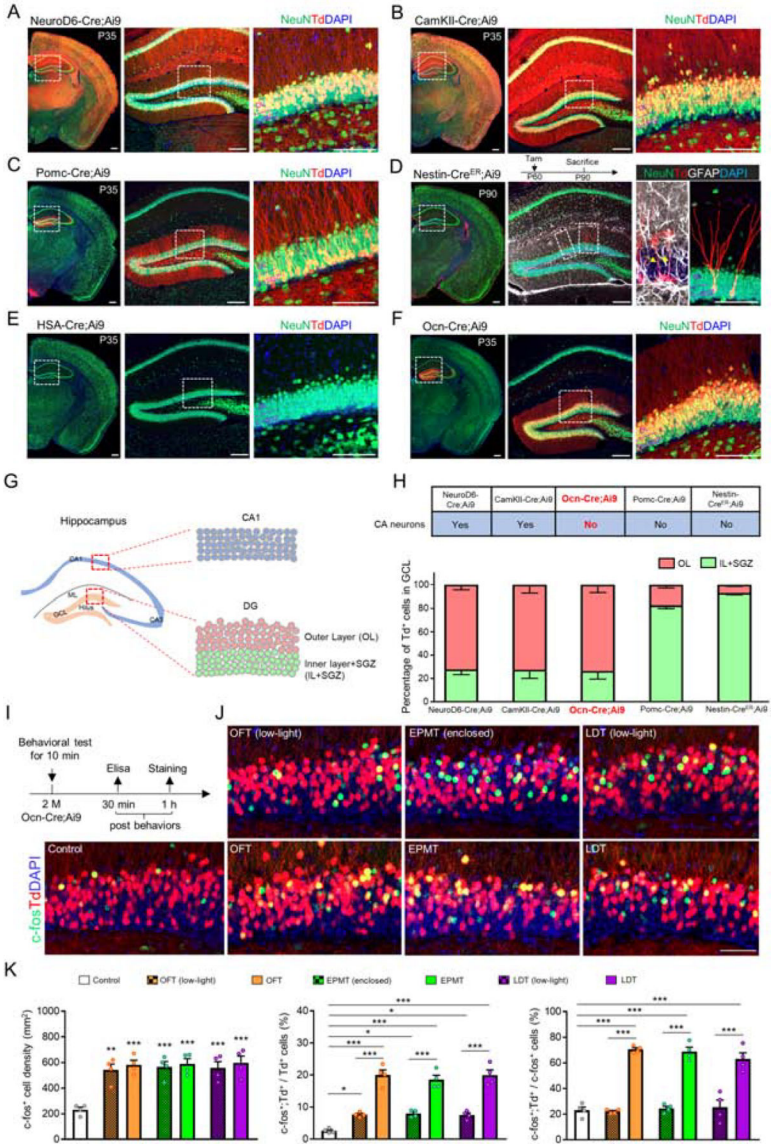

Figure 1. Screening for Cre lines that are positive in DGCs and responsive to anxiogenic environment

(A-F) Co-immunostaining analysis of NeuN (green) and Td (red) in brain sections from indicated mouse lines. A, Neurod6-Cre;Ai9 mouse; B, CamKII-Cre;Ai9 mouse; C, Pomc-Cre;Ai9 mouse; D, Nestin-Cre^{ER};Ai9 mouse. Arrows indicate GFAP^{+} (white) radial glia-like stem cells; E, HSA-Cre;Ai9 mouse; F, Ocn-Cre;Ai9 mouse. Higher magnification of the selected region in DG was shown beside each image. DAPI (blue) indicates cell nucleus. Scale bar = 100 μm.

(G) Schematic drawing shows the structure of adult mouse hippocampus, and the selected regions of CA1 and dDG were amplified.

(H) Summary of Cre expression in CA neurons of indicated mouse lines, and quantification of the percentage of Td^{+} neurons in different layers of dDG.

(I) Schematic diagram of behavioral tests in Ocn-Cre;Ai9 mice.

(J) Co-immunostaining analysis of c-fos (green) and Td (red) in dDG. DAPI (blue) indicates cell nucleus. Scale bar = 50 μm.

(K) Quantifications of the data in (J), the c-fos$^+$ cell density (left), the percentage of c-fos$^+$;Td$^+$/Td$^+$ cells (middle) and the percentage of c-fos$^+$;Td$^+$/c-fos$^+$ cells (right). n=4 for each group of mice. *p < 0.05; **p < 0.01; ***p < 0.001. One-way ANOVA followed by Tukey's post hoc test.

Data in (H and K) are presented as the mean ± SEM.

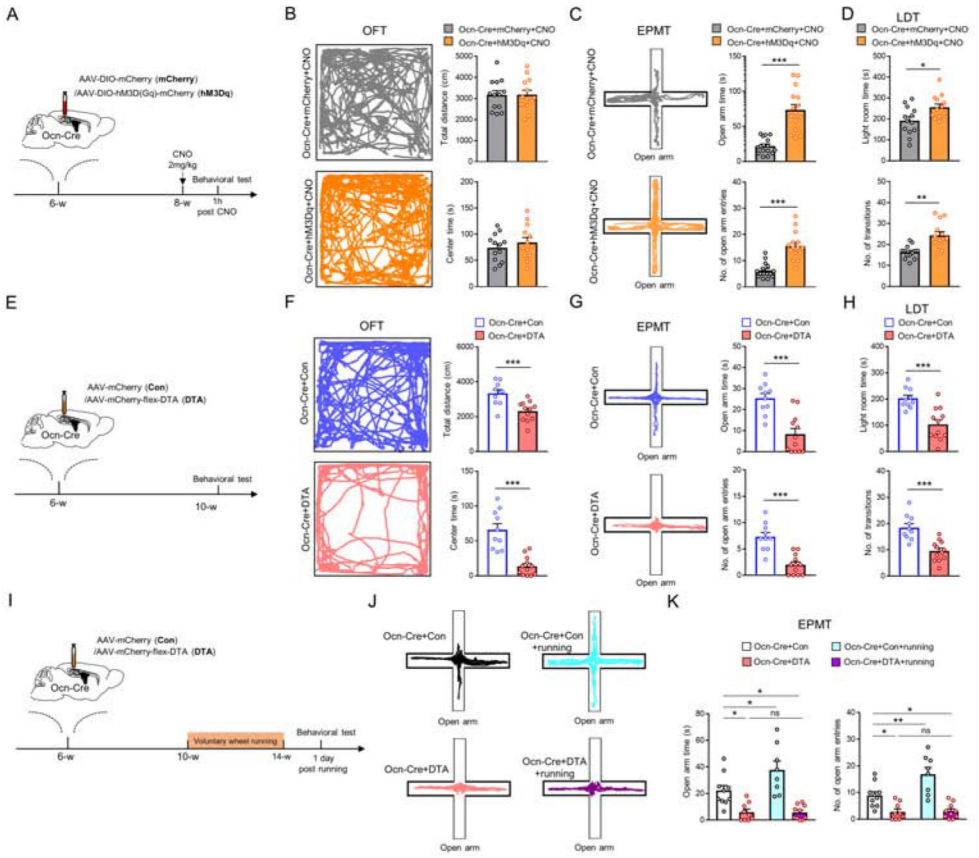

Figure 2. Suppression of anxiety-like behaviors by activating Ocn-Cre$^+$ dDGCs, whereas exacerbation of anxiety-like behaviors by ablating Ocn-Cre$^+$ dDGCs

(A) Schematic diagram of experimental design for behavioral tests in Ocn-Cre mice injected with AAV5-DIO-hM3Dq-mCherry or AAV5-DIO-mCherry. AAV5-DIO-hM3Dq-mCherry (hM3Dq) is a double floxed Gq-coupled hM3D DREADD AAV-virus, which expresses human synapsin promoter driven, Cre-dependent, hM3D(Gq) receptor with mCherry reporter. AAV5-DIO-mCherry (mCherry) is control.

(B) Representative tracing images and quantifications of total distance and center duration time in the OFT of Ocn-Cre+mCherry (n=13) and Ocn-Cre+hM3Dq (n=13) mice after CNO treatment.

(C) Representative tracing images and quantifications of open arm duration time and entries in the EMPT of Ocn-Cre+mCherry (n=15) and Ocn-Cre+hM3Dq (n=15) mice after CNO treatment. ***$p < 0.001$. Student's *t*-test.

(D) Quantifications of the time in the light room and the number of transitions into the light room of Ocn-Cre+mCherry (n=13) and Ocn-Cre+hM3Dq (n=13) mice after CNO treatment. *$p < 0.05$; **$p < 0.01$. Student's *t*-test.

(E) Schematic diagram of experimental design for behavioral tests in Ocn-Cre mice injected with Con or DTA viruses.

(F) Representative tracing images and quantifications of total distance and center duration time in the OFT of Ocn-Cre+Con (n=10) and Ocn-Cre+DTA (n=12) mice. ***$p < 0.001$. Student's *t*-test.

(G) Representative tracing images and quantifications of open arm duration time and entries in the EMPT of Ocn-Cre+Con (n=10) and Ocn-Cre+DTA (n=12) mice. ***p < 0.001. Student's *t*-test.

(H) Quantifications of the time in the light room and the number of transitions into the light room of Ocn-Cre+Con (n=10) and Ocn-Cre+DTA (n=12) mice. ***p < 0.001. Student's *t*-test.

(I) Schematic diagram of virus injections (control viruses or DTA) in Ocn-Cre mice and voluntary wheel running for behavioral test.

(J-K) Representative tracing images and quantifications of open arm duration time and entries in the EMPT of Ocn-Cre+Con and Ocn-Cre+DTA mice with or without running. Ocn-Cre+Con (n=10); Ocn-Cre+DTA (n=9); Ocn-Cre+Con+running (n=8); Ocn-Cre+DTA +running (n=10). *p < 0.05; **p < 0.01. Two-way ANOVA test for open arm time, interaction: $F_{(1, 33)}$=4.413, p=0.0434; running factor: $F_{(1, 33)}$=4.145, p=0.0499; virus factor: $F_{(1, 33)}$=40.88, p<0.0001. Two-way ANOVA test for open arm entries, interaction: $F_{(1, 33)}$=6.598, p=0.0149; running factor: $F_{(1, 33)}$=7.376, p=0.0104; virus factor: $F_{(1, 33)}$=43.9, p<0.0001.

Data in (B-D, F-H and K) are presented as the mean ± SEM.

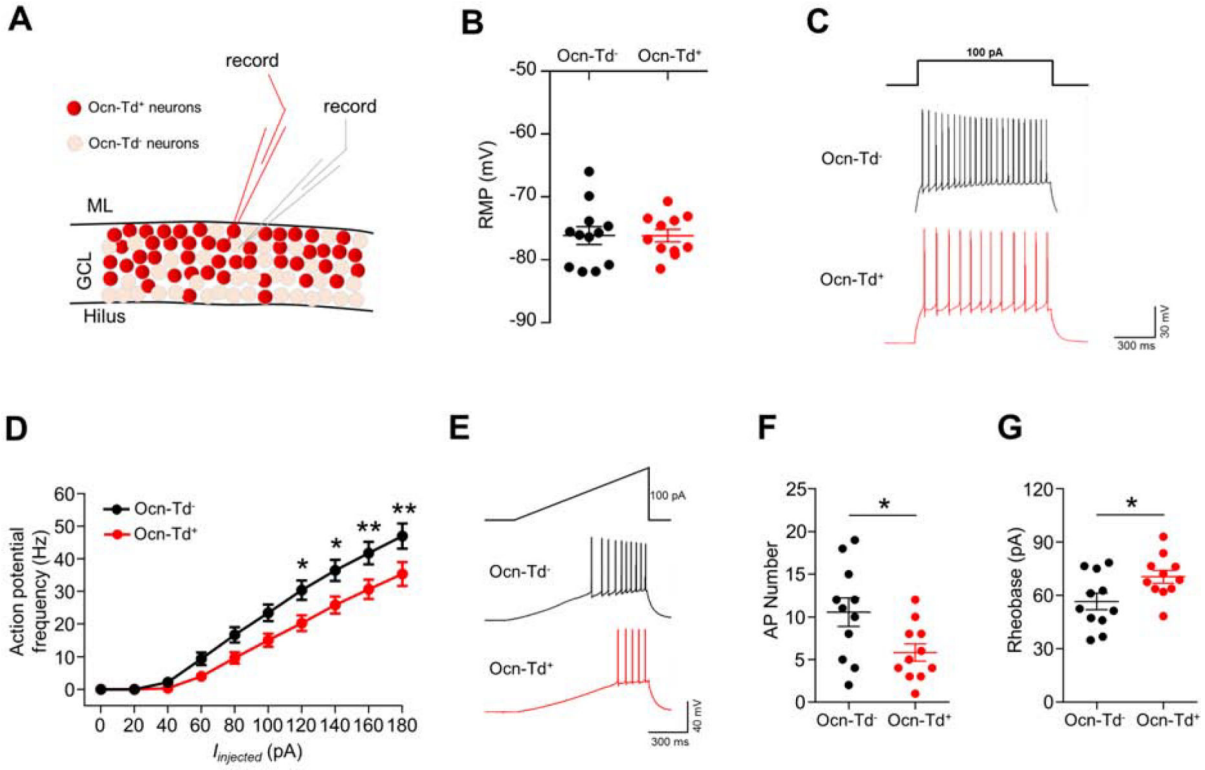

Figure 3. Lower excitability in Ocn-Cre^{+} dDGCs than that of neighboring Ocn-Cre^{-} dDGCs

(A) Schematic diagram of electrophysiological recordings in Ocn-Cre^{+} and neighbor Ocn-Cre^{-} dDGCs.

(B) Recordings of resting membrane potential (RMP) in Ocn-Cre^{+} (n=12) and neighbor Ocn-Cre^{-} (n=11) dDGCs.

(C) Representative action potential firing in DGCs evoked by a 100-pA depolarizing current pulse injection. Scale bar: 300 ms, 30 mV.

(D) Quantification of the mean frequency of action potential (AP) in response to different injected currents; n = 11 neurons in each group. *p < 0.05, **p < 0.01. Two-way ANOVA, interaction: $F_{(9, 200)}$=1.946, p=0.0475; injected currents factor: $F_{(9, 200)}$=89.75, p<0.0001; genotype factor: $F_{(1, 200)}$=40.52, p<0.0001.

(E) Representative action potential firing in DGCs evoked by a 100-pA depolarizing current ramp injection. Scale bar: 300 ms, 40 mV.

(F and G) Quantifications of AP numbers (F) and rheobase (G) in Ocn-Cre^{+} (n=11) and Ocn-Cre^{-} (n=11) dDGCs following a 100-pA depolarizing current ramp injection. *p < 0.05. Student's *t*-test.

Data in (B, D, F and G) are represented as the mean ± SEM.

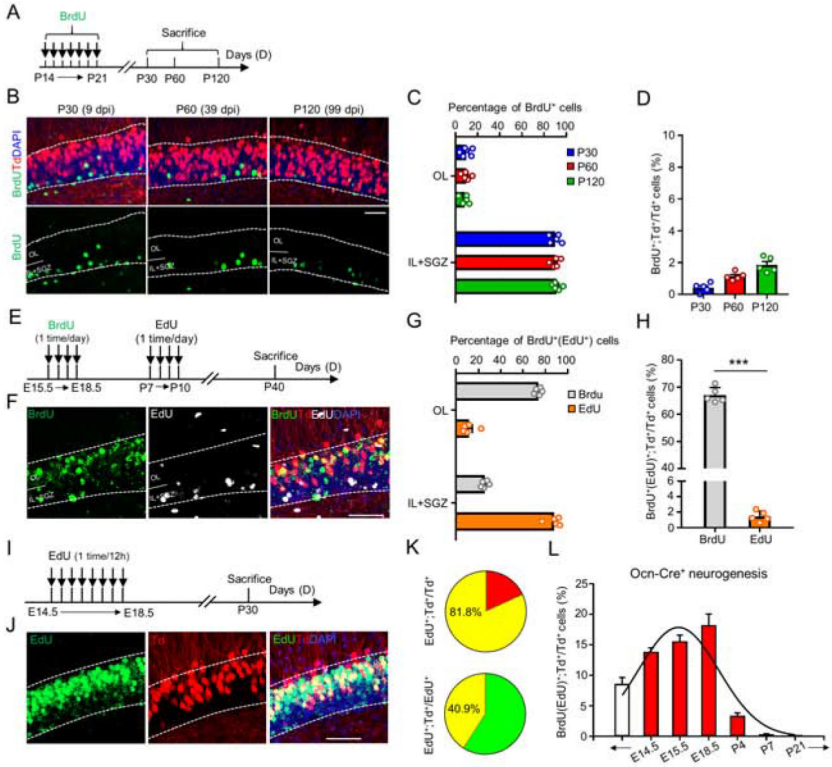

Figure 4. Ocn-Cre^{+} DGCs largely born in embryonic stages

(A) Schematic diagram of daily BrdU injections (P14-P21) and brains collection at indicated time.

(B) Co-immunostaining of BrdU (green) and Td (red) at indicated time in dDG. DAPI (blue) was stained for cell nucleus. Scale bar = 50μm.

(C) Quantification of the data in (B), the percentage of BrdU^{+} cells in different layers of dDG over total BrdU^{+} cells. n=5 in each group.

(D) Quantification of the data in (B), the percentage of BrdU^{+};Td^{+} cells over total Td^{+} cells. n=5 in each group.

(E) Schematic diagram of daily BrdU injections (E15.5 to E18.5) and daily EdU injections (P7 to P10) and brains collection at P40.

(F) Co-staining analysis of BrdU (green), Td (red), EdU (white) and DAPI (blue) in DG. Scale bar = 50μm. BrdU was detected immunochemically by using anti-BrdU antibody; EdU was detected by chemical staining with fluorescent dye.

(G) Quantification of the data in (F), the percentage of BrdU^{+} cells and EdU^{+} cells in different layers of dDG over total BrdU^{+} cells and EdU^{+} cells, respectively. n=5 in each group.

(H) Quantification of the percentage of BrdU^{+}(EdU^{+});Td^{+} cells over total Td^{+} cells in F. n=5 in each group. ***p < 0.001. Student's *t*-test.

(I) Schematic diagram of EdU injections (E14.5 to E18.5, 1 time/12h) and brains collection at P30.

(J) Co-staining analysis of EdU (green), Td (red) and DAPI (blue) in DG. Scale bar = 50μm.

(K) Quantification of the data in (J), the percentage of $EdU^+;Td^+$ cells over total Td^+ cells (top) and the percentage of $EdU^+;Td^+$ cells over total EdU^+ cells (bottom). n=4 mice.
(L) A summary of the Ocn-Cre^+ dDGCs generation throughout life.
Data in (C, D, G, H and L) are presented as the mean ± SEM.

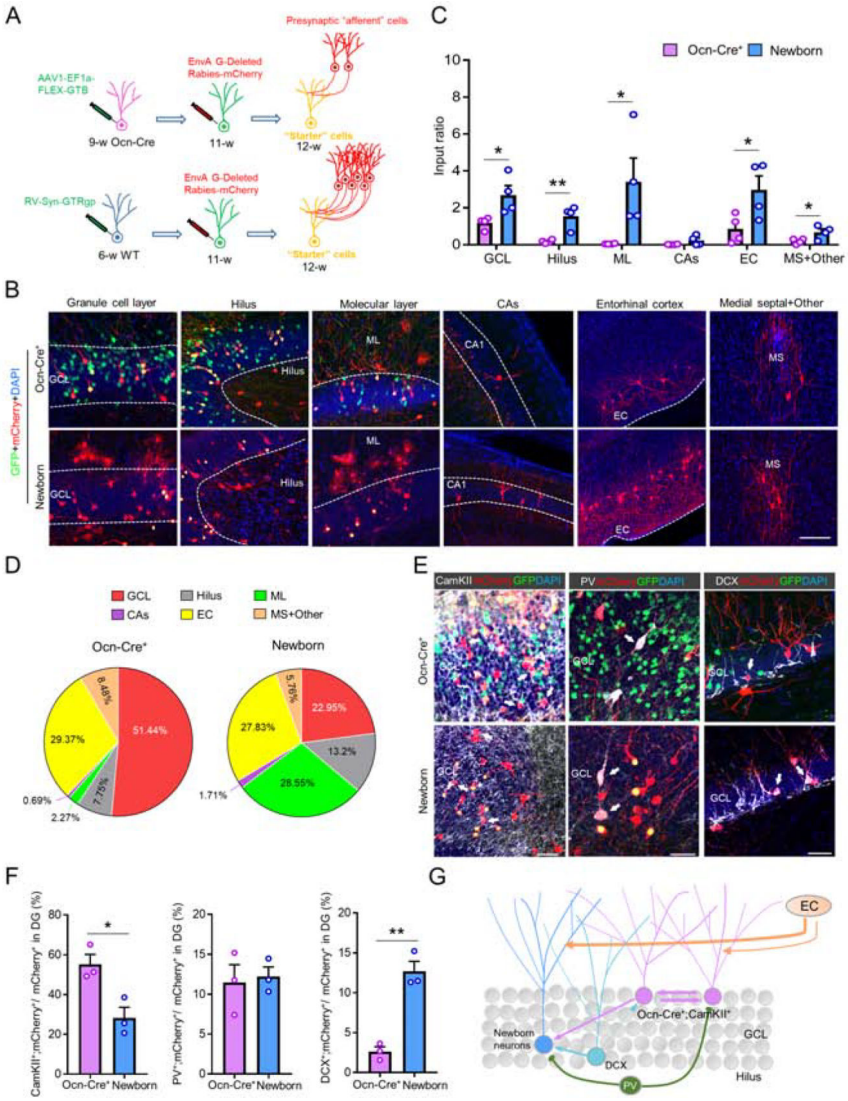

Figure 5. Less presynaptic inputs to Ocn-Cre$^+$ dDGCs than that of newborn dDGCs

(A) Schematic illustration of pseudotyped rabies virus-mediated monosynaptic retrograde tracing method. GFP$^+$;mCherry$^+$ (yellow) cells indicate "Starter" cells and mCherry$^+$ (red) cells indicate input cells.

(B) Representative image of input cells and starter cells in different brain regions. Granule cell layer (GCL); Molecular layer (ML); Entorhinal cortex (EC); Medial septal (MS). Scale bar = 50 μm.

(C) Quantification of the data in (B), the connectivity ratio (input cells over starter cells). *P < 0.05; **P < 0.01. Student's *t*-test. n=4 in each group.

(D) Quantification of the data in (B), the percentage of connectivity ratio from different brain regions.

(E) Co-immunostaining analyses of input cells (mCherry) with CaMKII, PV or DCX in DG. DAPI (blue) marks cell nucleus. White arrows indicate marker$^+$;mCherry$^+$ cells. Scale bar = 30 μm.

(F) Quantification of the data in (E), the percentage of $CaMKII^+$;$mCherry^+$, PV^+;$mCherry^+$ or DCX^+;$mCherry^+$ cells over $mCherry^+$ cells. *P < 0.05; **P < 0.01. Student's t-test. n=3 in each group.

(G) Illustration of the model of the presynaptic connectivity of Ocn-Cre^+ dDGCs and newborn dDGCs.

Data in (C and F) are presented as the mean ± SEM.

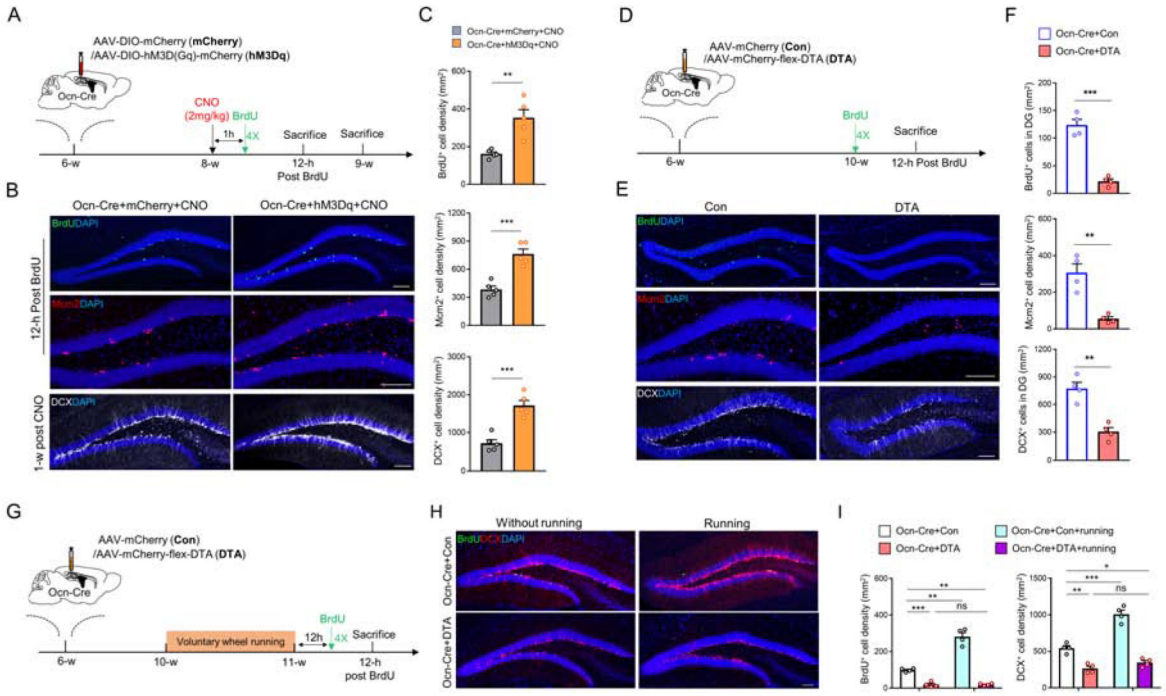

Figure 6. Increased adult DG neurogenesis by activating Ocn-Cre$^+$ dDGCs, whereas decreased adult DG neurogenesis by ablating Ocn-Cre$^+$ dDGCs

(A) Schematic diagram of experimental design for analysis of adult DG neurogenesis following activating Ocn-Cre$^+$ dDGCs.

(B) Representative images of BrdU (green), Mcm2 (red) and DCX (white) in Ocn-Cre +mCherry+CNO and Ocn-Cre+hM3Dq+CNO mice. DAPI (blue) indicate cell nucleus. Scale bar = 100 μm.

(C) Quantitative analyses of the data in (B), the density of BrdU$^+$ (top), Mcm2$^+$ (middle) and DCX$^+$ (bottom) cells. **p < 0.01. ***p < 0.001. Student's *t*-test. n=5 in each group.

(D) Schematic diagram of experimental design for analysis of adult DG neurogenesis following deleting Ocn-Cre$^+$ dDGCs.

(E) Representative images of BrdU (green), Mcm2 (red) and DCX (white) in Ocn-Cre+Con and Ocn-Cre+DTA mice. DAPI (blue) indicates cell nucleus. Scale bar = 100 μm.

(F) Quantitative analyses of the data in (E), the density of BrdU$^+$ (top), Mcm2$^+$ (middle) and DCX$^+$ (bottom). **p < 0.01. ***p < 0.001. Student's *t*-test. n=4 in each group.

(G) Schematic diagram of virus injections (control viruses or DTA) in dDG and voluntary wheel running for analyzing adult DG neurogenesis.

(H) Co-immunostaining analysis of BrdU (green) and DCX (red) in DG of Ocn-Cre+Con and Ocn-Cre+DTA mice with or without running. DAPI (blue) indicates cell nucleus. Scale bar = 100 μm.

(I) Quantifications of the data in (H), the density of Brdu$^+$ (left) cells and DCX$^+$ (right) cells. n=4 mice in each group. *p < 0.05; **p < 0.01; ***p < 0.001. Two-way ANOVA test for BrdU$^+$ cell density, interaction: $F_{(1, 12)}$=58.8, p<0.0001; running factor: $F_{(1, 12)}$=59.77, p<0.0001; virus factor: $F_{(1, 12)}$=206.1, p<0.0001. Two-way ANOVA test for DCX$^+$ cell density, interaction: $F_{(1, 12)}$=25.06, p=0.0003; running factor: $F_{(1, 12)}$=50.54, p<0.0001; virus factor: $F_{(1, 12)}$=151, p<0.0001.

Data in (C, F and I) are presented as the mean ± SEM.

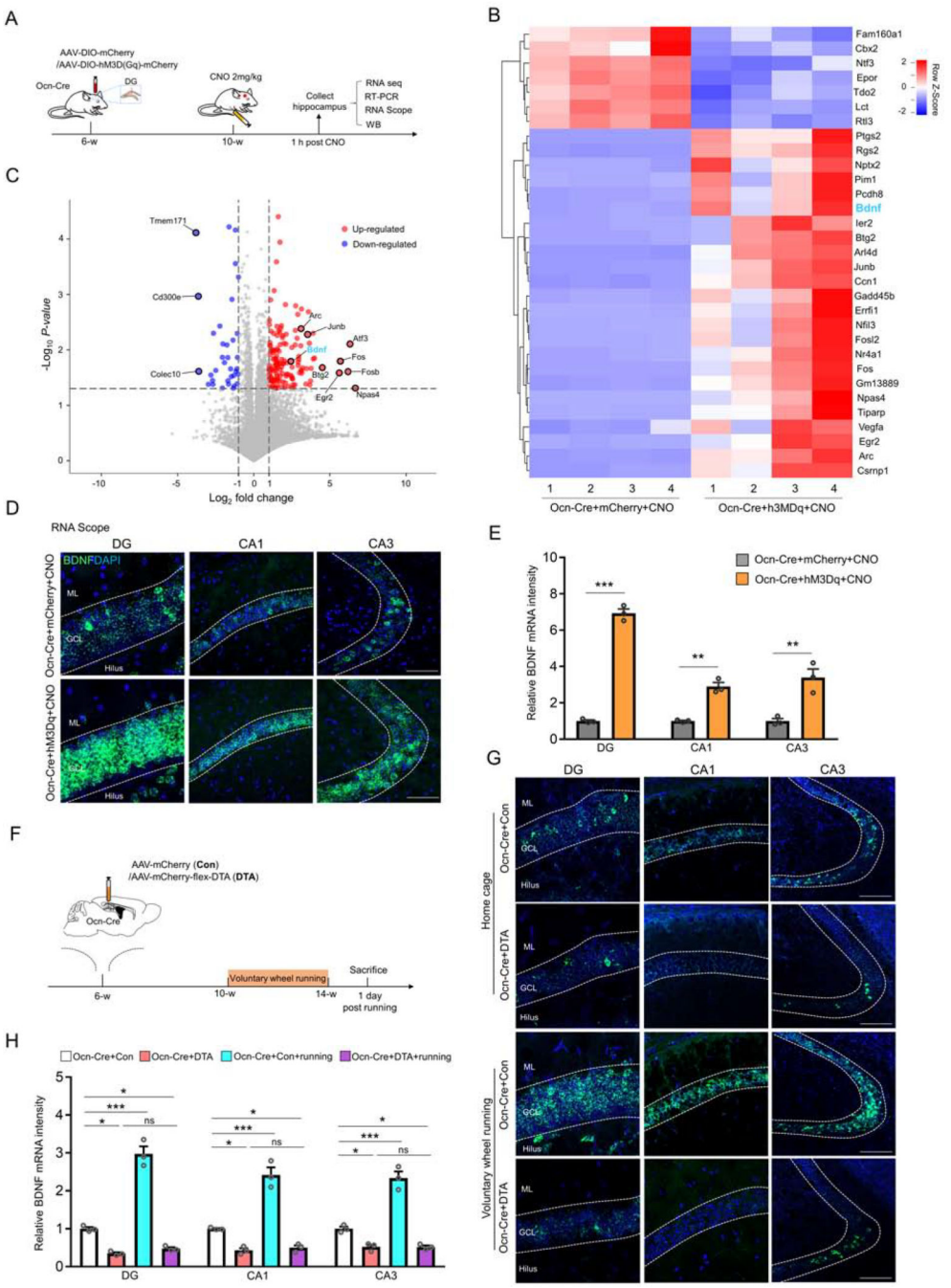

Figure 7. Ocn-Cre^{+} DGCs, a key cellular source for neuronal activity induced BDNF expression

(A) Schematic diagram of experimental design in Ocn-Cre mice expressing mCherry or hM3Dq. The Ocn-Cre mice injected with mCherry or hM3Dq viruses into their dDGs (at 6-weeks old) were treated with CNO (2mg/kg) (at 8-week old) for 1 h, and their hippocampi were then subjected to RNA-seq analyses, RT-PCR, RNA scope and Western blot.

(B and C) Heat map (B) and Volcano plots (C) of differentially expressed genes identified by RNA-seq in Ocn-Cre+hM3Dq+CNO mice over Ocn-Cre+mCherry+CNO mice.

(D) Detection of BDNF mRNA by RNA scope in DG, CA1 and CA3 of Ocn-Cre+hM3Dq +CNO and Ocn-Cre+mCherry+CNO mice. Scale bar = 100 μm.
(E) Quantification of the data in (D), the relative BDNF mRNA level. **p < 0.01. ***p < 0.001. Student's *t*-test. n=3 mice in each group.
(F) Schematic diagram of virus injections (control viruses or DTA) in Ocn-Cre mice and voluntary wheel running.
(G) Detection of BDNF mRNA by RNA scope in DG, CA1 and CA3 of Ocn-Cre+Con and Ocn-Cre+DTA mice with or without voluntary wheel running. Scale bar = 100 μm.
(H) Quantifications of the data in (G), the relative BDNF mRNA level. *p < 0.05; ***p < 0.001. n=3 mice in each group. Two-way ANOVA test. For DG region, interaction: $F_{(1, 8)}$=76.96, p<0.0001; running factor: $F_{(1, 8)}$=99.37, p<0.0001; virus factor: $F_{(1, 8)}$=223, p<0.0001. For CA1 region, interaction: $F_{(1, 8)}$=37.64, p=0.0003; running factor: $F_{(1, 8)}$=45.87, p=0.0001; virus factor: $F_{(1, 8)}$=128.1, p<0.0001. For CA3 region, interaction: $F_{(1, 8)}$=45.65, p=0.0001; running factor: $F_{(1, 8)}$=45.47, p=0.0001; virus factor: $F_{(1, 8)}$=134.4, p<0.0001.
Data in (E and H) are presented as the mean ± SEM.

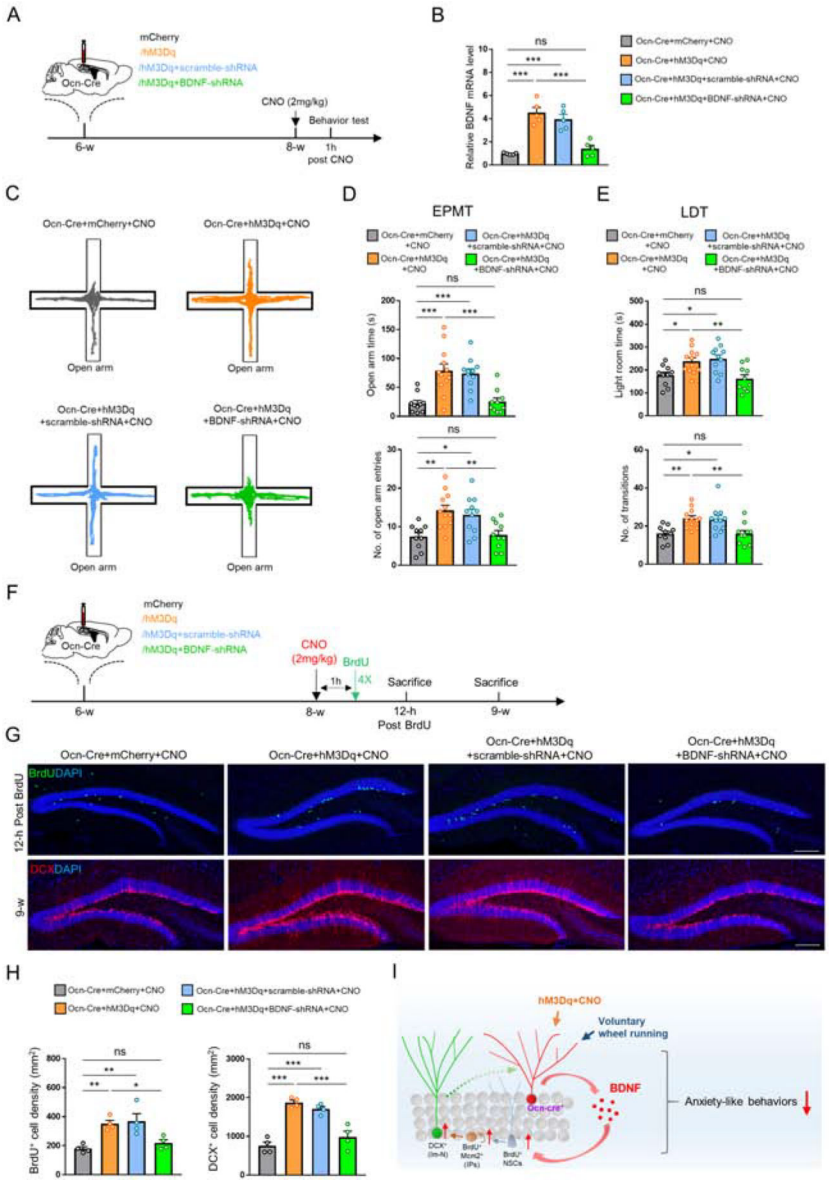

Figure 8. Requirement of BDNF in hippocampus for activation of Ocn-Cre^{+} dDGCs to suppress anxiety-like behaviors and promote adult DG neurogenesis

(A) Schematic diagram of virus injections (mCherry, hM3Dq, hM3Dq+scramble-shRNA or hM3Dq+BDNF-shRNA) in Ocn-Cre mice for behavioral tests.

(B) RT-PCR analysis of relative BDNF mRNA level in hippocampus of Ocn-Cre mice injected with indicated viruses. ***p < 0.001. ns = no significant difference. One-way ANOVA followed by Tukey's post hoc test. n=5 in each group.

(C-D) Representative tracing images and quantifications of open arm duration time and entries in the EMPT of each group of mice after CNO treatment. *p < 0.05; **p < 0.01; ***p < 0.001. ns = no significant difference. One-way ANOVA followed by Tukey's post hoc test. Ocn-Cre+mCherry+CNO (n=10); Ocn-Cre+hM3Dq+CNO (n=12); Ocn-Cre +hM3Dq+scramble-shRNA+CNO (n=11); Ocn-Cre+hM3Dq+BDNF-shRNA+CNO (n=10).

(E) Quantifications of the time in the light room and the number of transitions into the light room of each group of mice. *p < 0.05; **p < 0.01. ns = no significant difference. One-way ANOVA followed by Tukey's post hoc test. Ocn-Cre+mCherry (n=10); Ocn-Cre+hM3Dq (n=12); Ocn-Cre+hM3Dq+scramble shRNA (n=11); Ocn-Cre+hM3Dq+BDNF shRNA (n=10).

(F) Schematic diagram of virus injections (mCherry, hM3Dq, hM3Dq+scramble-shRNA or hM3Dq+BDNF-shRNA) in Ocn-Cre mice for analyzing adult DG neurogenesis.

(G) Immunostaining of BrdU (green) and DCX (red) in DG of Ocn-Cre mice injected with indicated viruses after CNO treatment. Scale bar = 100 μm.

(H) Quantifications of the data in (G), the density of $Brdu^+$ (left) and DCX^+ (right) cells. *p < 0.05; **p < 0.01; ***p < 0.001. ns = no significant difference. One-way ANOVA followed by Tukey's post hoc test. n = 4 mice in each group.

(I) Summary of results and a working model for Ocn-Cre^+ dDGCs to regulate anxiety-like behaviors and adult DG neurogenesis.

Data in (B, D, E and H) are presented as the mean ± SEM.

KEY RESOURCES TABLE

Resource Type	Specific Reagent or Resource	Source or Reference	Identifiers	Additional Information
Add additional rows as needed for each resource type	Include species and sex when applicable.	Include name of manufacturer, company, repository, individual, or research lab. Include PMID or DOI for references; use “this paper” if new.	Include catalog numbers, stock numbers, database IDs or accession numbers, and/or RRIDs. RRIDs are highly encouraged; search for RRIDs at https://scicrunch.org/resources.	Include any additional information or notes if necessary.
Antibody	mouse anti-Akt1/2/3	Santa Cruz	sc-81434; RRID:AB_1118808	
Antibody	mouse anti-p-Akt1/2/3	Santa Cruz	sc-514032	
Antibody	rabbit anti-Erk1/2	Cell Signaling	Cat# 9102S; RRID:AB_330744	
Antibody	rabbit anti-p-Erk1/2	Cell Signaling	Cat# 4370S; RRID:AB_2315112	
Antibody	mouse anti-c-fos	Santa Cruz	sc-271243; RRID:AB_10610067	
Antibody	mouse anti-Mcm2	BD Biosciences	Cat# 610700; RRID:AB_2141952	
Antibody	goat anti-DCX	Santa Cruz	sc-8066; RRID:AB_2088494	
Antibody	mouse anti-NeuN	Millipore	MAB377; RRID:AB_2298772	
Antibody	rat anti-BrdU	Accurate chemical & scientific corporation	OBT0030; RRID:AB_609568	
Antibody	chicken anti-GFP	aves	Cat# GFP-1020, RRID:AB_10000240	
Antibody	rabbit anti-mCherry	Takara	Cat# 632496, RRID:AB_10013483	
Antibody	mouse anti-CamKII	Cell Signaling	Cat# 50049, RRID:AB_2721906	
Antibody	goat anti-TrkB	R&D systems	Cat# AF1494-SP	
Antibody	rabbit anti-p-TrkB	Millipore	Cat# ABN1381, RRID:AB_2721199	
Antibody	rabbit anti-BDNF	Millipore	Cat# AB1779SP, RRID:AB_90994	
Antibody	mouse anti-β-actin	Abcam	Cat# ab8227, RRID:AB_2305186	
Chemical Compound or Drug	5-Bromo-2’-deoxyuridine (BrdU)	Sigma	Cat# B5002	
Chemical Compound or Drug	5-ethynyl-2’-deoxyuridine (EdU)	ABP Biosciences	Cat# A012	
Chemical Compound or Drug	Tamoxifen	Sigma	Cat# T5648	
Chemical Compound or Drug	Clozapine-N-oxide (CNO)	Sigma	Cat# C0832	
Commercial Assay Or Kit	Corticosterone ELISA kit	Abcam	Cat# ab108821	
Bacterial or Viral Strain	AAV-hSyn-DIO-mCherry	Addgene	Cat# 50459	
Bacterial or Viral Strain	AAV-hSyn-DIO-hM3D(Gq)-mCherry	Addgene	Cat# 44361	
Bacterial or Viral Strain	AAV-hSyn-DIO-hM4D(Gi)-mCherry	Addgene	Cat# 44362	

Resource Type	Specific Reagent or Resource	Source or Reference	Identifiers	Additional Information
Bacterial or Viral Strain	AAV-mCherry-flex-DTA	UNC Vector Core		
Bacterial or Viral Strain	Lenti-scramble shRNA	Origene	Cat# TR30021V	
Bacterial or Viral Strain	Lenti-BDNF shRNA	Origene	Cat# TL513468V	
Organism/Strain	Mouse: CD-1	Charles river		
Organism/Strain	Mouse: Ocn-Cre	provided by T. Clemens (Johns Hopkins Medical School, Baltimore, MD) and X. Shi (Augusta University, Augusta, GA)		
Organism/Strain	Mouse: Neurod6-Cre	provided by Dr. KA Nave		
Organism/Strain	Mouse: CaMKII-Cre	The Jackson Laboratory	Stock# 005359	
Organism/Strain	Mouse: Pomc-Cre	The Jackson Laboratory	Stock# 005965	
Organism/Strain	Mouse: HSA-Cre	The Jackson Laboratory	Stock# 006149	
Organism/Strain	Mouse: NestinCreERT2	The Jackson Laboratory	Stock# 016261	
Organism/Strain	Mouse: Ai3	The Jackson Laboratory	Stock# 007903	
Organism/Strain	Mouse: Ai9	The Jackson Laboratory	Stock# 007907	